JOC The Journal of Organic Chemistry

Article

pubs.acs.org/joc

Mechanistic Insights into the Directed Hydrogenation of Hydroxylated Alkene Catalyzed by Bis(phosphine)cobalt Dialkyl Complexes

Xuelu Ma[†,‡] and Ming Lei*[,†]

[†]State Key Laboratory of Chemical Resource Engineering, Institute of Materia Medica, College of Science, Beijing University of Chemical Technology, Beijing 100029 P. R. China

[‡]Department of Chemistry and Key Laboratory of Organic Optoelectronics & Molecular Engineering of Ministry of Education, Tsinghua University, Beijing 100084, P. R. China

Supporting Information

ABSTRACT: The mechanism of directed hydrogenation of hydroxylated alkene catalyzed by bis(phosphine)cobalt dialkyl complexes has been studied by DFT calculations. The possible reaction channels of alkene hydrogenation catalyzed by catalytic species ($\mathbf{0_T}$, $\mathbf{0_P}$, and $\mathbf{0}$) were investigated. The calculated results indicate that the preferred catalytic activation processes undergo a 1,2 alkene insertion. $\mathbf{0_P}$ and $\mathbf{0}$ prefer the β hydrogen elimination mechanism with an energy barrier of 9.5 kcal/mol, and $\mathbf{0_T}$ prefers the reductive elimination mechanism with an energy barrier of 11.0 kcal/mol. The second H_2 coordination in the σ bond metathesis mechanism needs to break the agostic H^2–βC bond of metal–alkyl intermediates ($\mathbf{2_{1P}}$ and $\mathbf{2_{1T}}$), which owns the larger energetic span compared to the reductive elimination. This theoretical study shows that the most favorable reaction pathway of alkene hydrogenation is the β hydrogen elimination pathway catalyzed by the planar (dppe)CoH_2. The hydrogenation activity of Co(II) compounds with redox-innocent phosphine donors involves the Co(0)–Co(II) catalytic mechanism.

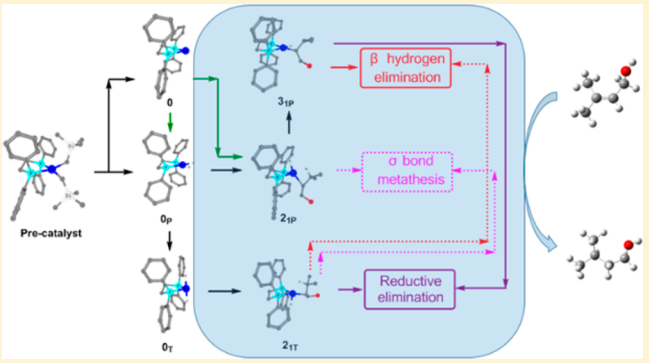

INTRODUCTION

The catalytic hydrogenation of unsaturated compounds is one of the earliest research fields in homogeneous catalysis. Exploring the most effective methods for the preparation of single enantiomer compounds is a growing field, especially in the pharmaceutical and agrochemical industries.[1,2] Whereas traditional homogeneous asymmetric hydrogenation catalysts are based on precious metals, such as iridium, rhodium, and ruthenium, there is an increase in efforts to develop catalysts based on more abundant metals.[3] Catalysts containing iron and cobalt are attractive candidates due to their obvious advantages of being easily accessible, versatile, and environmentally friendly. Cobalt-containing complexes have been reported as effective catalysts for homogeneous hydrogenation. Studies by Pregaglia,[4] Ohgo,[5] Pfaltz,[6] Corma,[7] Shainyan,[8] Budzelaar,[9] Chirik,[10] Hanson,[11] and Peters[12] were reported to support the potential of ligand-assisted cobalt complex for the catalytic hydrogenation of olefinic compounds.

Chirik et al. devised a high-throughput process to develop a class of highly enantioselective cobalt-based hydrogenation catalysts containing chiral bidentate bis(phosphines) for the hydrogenation of both functionalized and unfunctionalized alkene substrates.[13] Later, achiral analogues of these complexes with readily available bidentated phosphine ligands were reported for the directed hydrogenation of hydroxylated alkenes as shown in Scheme 1, which features exclusively metal-centered reactivity with cobalt.[14] Unlike those in precious metal chemistry, most base metal alkene hydrogenation catalysts are readily deactivated by acidic hydroxyl functionality.[15] The mechanism for alkene hydrogenation catalyzed by the planar, low-spin bis(phosphine)cobalt(II) dialkyl complexes involves initial hydrogenolysis of the alkyl groups to release $SiMe_4$ observed by NMR spectroscopy, but the geometry of (diphosphine)CoH_2 is still unknown, which also makes details of the subsequent alkene insertion and catalyst regeneration uncertain. Due to the inherent thermal instability of Co–(H_2),

Scheme 1. Directed Alkene Hydrogenation with Bis(phosphine)cobalt Dialkyl Complexes

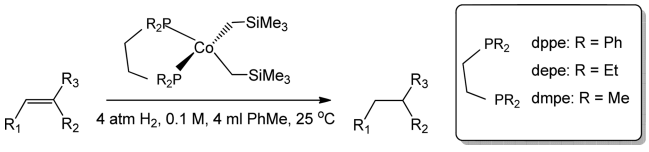

Received: January 4, 2017
Published: February 14, 2017

DOI: 10.1021/acs.joc.7b00016
J. Org. Chem. 2017, 82, 2703–2712

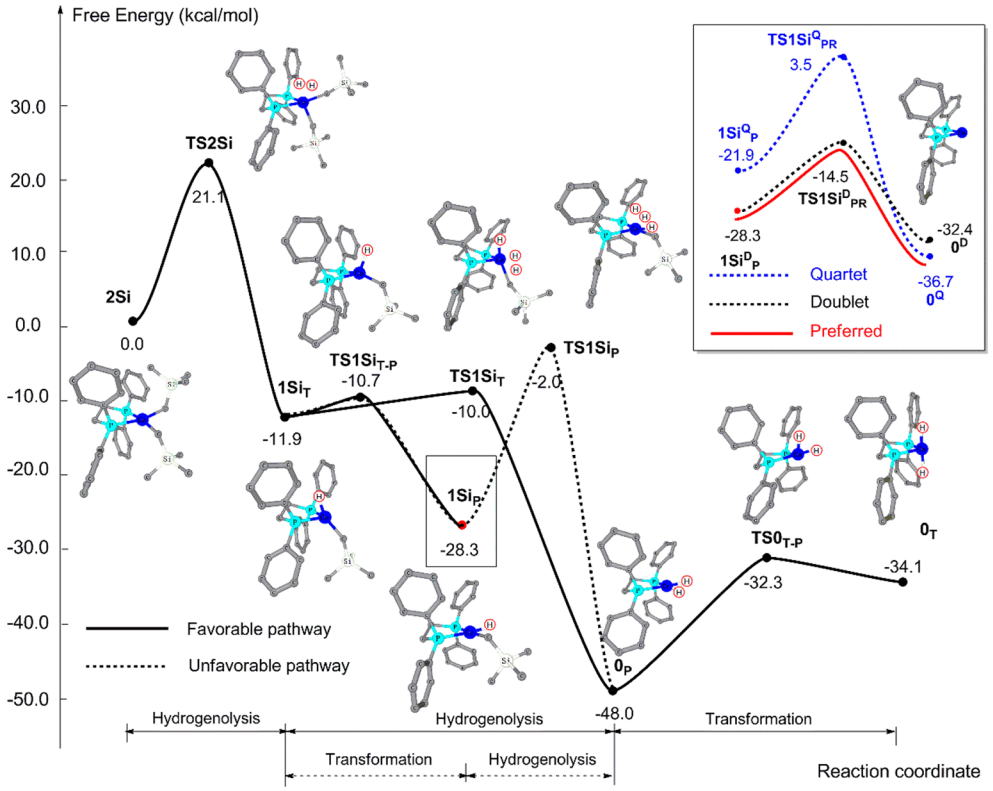

Figure 1. Free energy profiles of initial hydrogenolysis of bis(phosphine) cobalt(II) dialkyl complex (**2Si**) (H atoms are partly hidden, energy units: kcal/mol).

there are few studies of its use in catalytic transformations.[16] The existence of Co(0) species was provided by the isolation of (dppe)Co(COD), and it is important to unveil the nature of Co(0) species formation and catalytic activation in this system.

Intrigued by the various pathways of alkene hydrogenation and high efficiency of this catalytic system, herein we used a density functional theory (DFT) calculation to elucidate the catalytic mechanism of the directed hydrogenation of hydroxylated alkene (3-methylbut-2-en-1-ol) catalyzed by bis(phosphine)cobalt dialkyl complexes. In this study, we focused on the following critical issues: (i) the initial species of the catalytic activation and possible reaction channels; (ii) the alkene regioselectivity of 1,2 insertion vs 2,1 insertion; (iii) mechanisms involving reductive elimination, σ bond metathesis, and β elimination; and (iv) the preferred catalytic activation process. To the best of our knowledge, this is the first detailed theoretical study on the mechanism of the directed hydrogenation of hydroxylated alkene catalyzed by bis(phosphine) cobalt dialkyl complexes.

COMPUTATIONAL METHODS

All calculations were performed on experimental full-size dppe systems using the Gaussian 09 program package.[17] The geometries of all structures reported in this paper were optimized without any symmetry constraint at the B3LYP/BSI level. BSI was denoted as the effective core potential by Hay and Wadt with a double-ζ basis set (Lanl2dz) for Co and 6-31G* for all of the other atoms.[18] The B3LYP method was found to be reliable for the catalytic mechanistic studies of the transition-metal complexes.[19] In order to verify the reliability of use of the B3LYP method, all structures in the first part of the initiation of active species were also reoptimized with a suitable dispersion corrected functional (ωB97X-D) as shown in Figure S1 and Table S1. Frequency calculations were carried out for each transition state (**TS**) owning one imaginary frequency. Intrinsic reaction coordinate calculations along the whole pathway were performed in order to unveil more details around transition states and the corresponding intermediates. Atomic polar tensor charges are presented to describe the charge population because experimental evaluation of density functional charge schemes found that the commonly used Mulliken charge analysis was generally deficient.[20] The polarizable continuum model[21] was employed to compute potential energy (E_{sol}^{pot}) and nonelectrostatic interaction energy ($\Delta E_{nonelect}$) in the solvent (toluene) where gas-phase optimized structures were employed. The Gibbs energy (G_{sol}^0) in toluene is provided to discuss the reaction profile. In a bimolecular process, such as the alkene coordination and H_2 addition, the entropy change must be taken into consideration because the entropy considerably decreases in the process. In this case, G_{sol}^0 must be evaluated as follows

$$\begin{aligned} G_{sol}^0 &= H_0 - T(S_r^0 + S_v^0 + S_t^0) \\ &= ET + P\Delta V - T(S_r^0 + S_v^0 + S_t^0) \\ &= E_{sol} + E_{therm} - T(S_r^0 + S_v^0 + S_t^0) \\ &= E_{gas}^{v_0} + E_{sol}^{pot} + E_{nonelect} + E_{therm} - T(S_r^0 + S_v^0 + S_t^0) \end{aligned}$$

where ΔV is 0 in solution, E_{sol} is the potential energy with zero-point energy correction in solvent, $E_{gas}^{v_0}$ represents the zero-point vibrational energy in the gas phase, E_{therm} is the thermal correction by translational, vibrational, and rotational movements, and S_r^0, S_v^0 and S_t^0 are rotational, vibrational, and translational entropies, respectively. In general, the Thacker–Tetrode equation is used to evaluate translational entropy S_t^0. In solution, however, the usual Thacker–Tetrode equation cannot be directly applied to the evaluation of S_t^0 because S_t^0 is suppressed very much in solution.[22] In this context, we evaluated the translational entropy with the method by developed by Whitesides et al.[23] All corrected Gibbs energies calculated at 298.15 K were shown in the energy profile discussed below. For each minimum, doublet and quartet spin states have been considered, and the doublet spin states are always the most stable by 3–10 kcal/mol except for

DOI: 10.1021/acs.joc.7b00016
J. Org. Chem. 2017, 82, 2703–2712

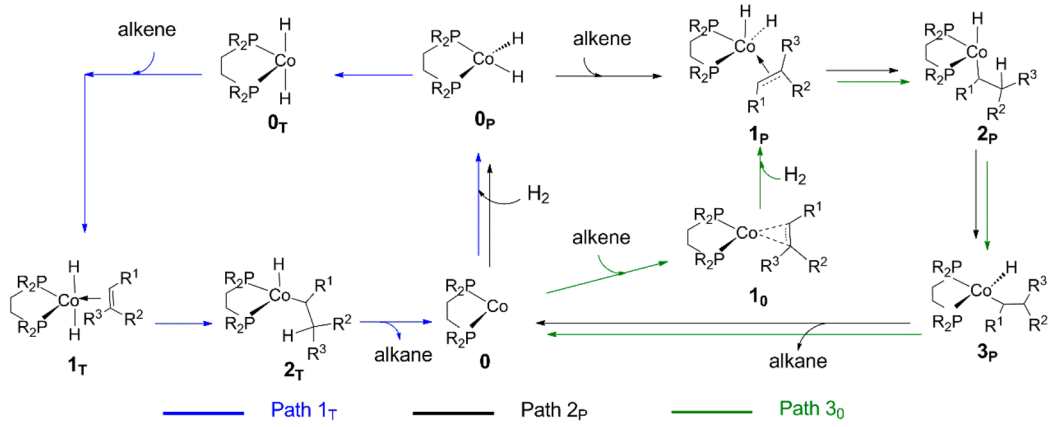

Figure 2. Proposed reductive elimination mechanism for the alkene hydrogenation catalyzed by bis(phosphine)cobalt complexes.

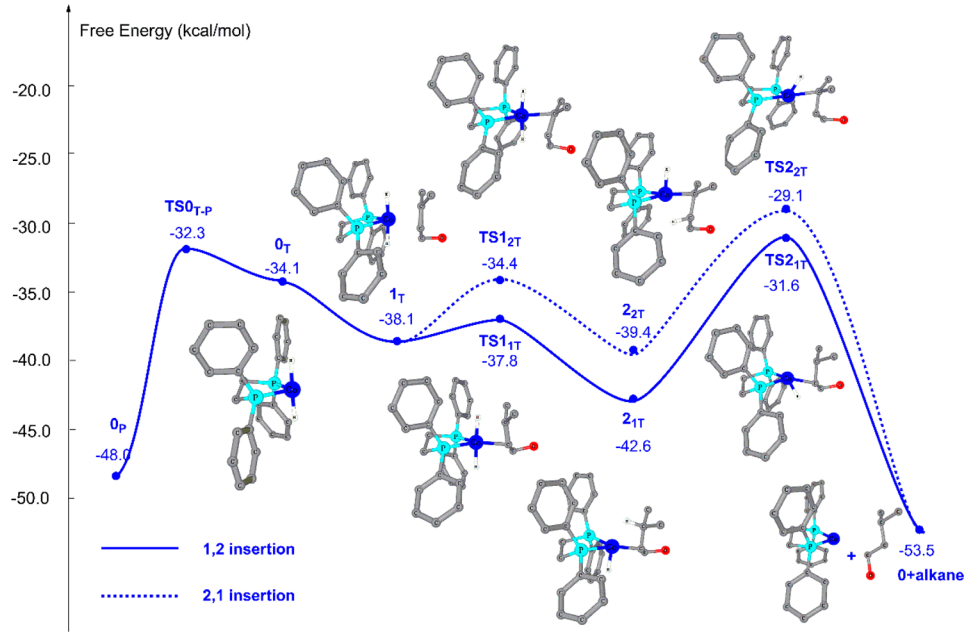

Figure 3. Free energy profiles of the reductive elimination mechanism for prenyl alcohol hydrogenation catalyzed by the vertical (dppe)CoH_2, $\mathbf{0_T}$ (path 1_T) (H atoms are partly hidden, energy units: kcal/mol).

bis(phosphine)cobalt(0) complex **0**. All relative energies of stationary points along the reaction pathway are relative to **2Si** ((dppe)Co-$(CH_2SiMe_3)_2$). The Cartesian coordinates of all optimized structures are presented in the Supporting Information.

RESULTS AND DISCUSSION

Initiation of the Active Species. The beginning of our investigation focused on the hydrogenolysis of the precatalyst **2Si**, (dppe)$Co(CH_2SiMe_3)_2$. The mechanism and corresponding energy profiles for alkene hydrogenation catalyzed by the planar, low-spin bis(phosphine)cobalt(II) dialkyl complexes involves initial hydrogenolysis of the alkyl groups to release $SiMe_4$ as shown in Figure 1. To give the first $SiMe_4$, a metathesis-type proton transfers to form Co−H in $\mathbf{1Si_T}$ with a barrier of 21.1 kcal/mol via **TS2Si**, which is exergonic by 33.0 kcal/mol to form the vertical hyride complex $\mathbf{1Si_T}$. To perform the second hydrogenolysis, two possible pathways lead to the active species ((dppe)CoH_2, such as $\mathbf{0_P}$, $\mathbf{0_T}$): the first pathway is shown by a dashed line via a geometrical transformation from the vertical $\mathbf{1Si_T}$ to the planar $\mathbf{1Si_P}$ ($\mathbf{1Si_T} \rightarrow \mathbf{1Si_P} \rightarrow \mathbf{0_P} \rightarrow \mathbf{0_T}$); the second pathway is shown by a solid line via a direct hydrogenolysis from $\mathbf{1Si_T}$ to $\mathbf{0_P}$ with a realizable energy barrier of 1.9 kcal/mol ($\mathbf{1Si_T} \rightarrow \mathbf{0_P} \rightarrow \mathbf{0_T}$). In the first pathway, although the geometrical transformation from the vertical $\mathbf{1Si_T}$ to the planar $\mathbf{1Si_P}$ owns a facile energy barrier of 1.2 kcal/mol and planar $\mathbf{1Si_P}$ is more stable than $\mathbf{1Si_T}$, it is very difficult for $\mathbf{1Si_P}$ to form $\mathbf{0_P}$ with an energy barrier of 26.3 kcal/mol. Therefore, the active (diphosphine)CoH_2 is the most possibly obtained from two successive hydrogenolyses without geometrical transformation, and the planar dihyride complex $\mathbf{0_P}$ is presumed to be not the only active species in the catalytic reaction, which could transform into the vertical $\mathbf{0_T}$ via $\mathbf{TS0_{T-P}}$ with a barrier of 15.7 kcal/mol. Both hydrogenolysis products of (diphosphine)$Co(CH_2SiMe_3)_2$, $\mathbf{0_T}$ and $\mathbf{0_P}$, as well as the intermediates in the hydrogenolysis process are the most stable initial active species on the doublet surface. Exceptionally, bis(phosphine) cobalt(0) complex **0** on the quartet surface as its ground state is generated from reductive elimination of $\mathbf{1Si_P}$ on the doublet with a barrier of 13.8 kcal/mol, and the energy of **0** on the doublet state ($\mathbf{0^D}$) is 4.3 kcal/mol higher than **0** on the quartet state ($\mathbf{0^Q}$). The energies of products of

DOI: 10.1021/acs.joc.7b00016
J. Org. Chem. 2017, 82, 2703−2712

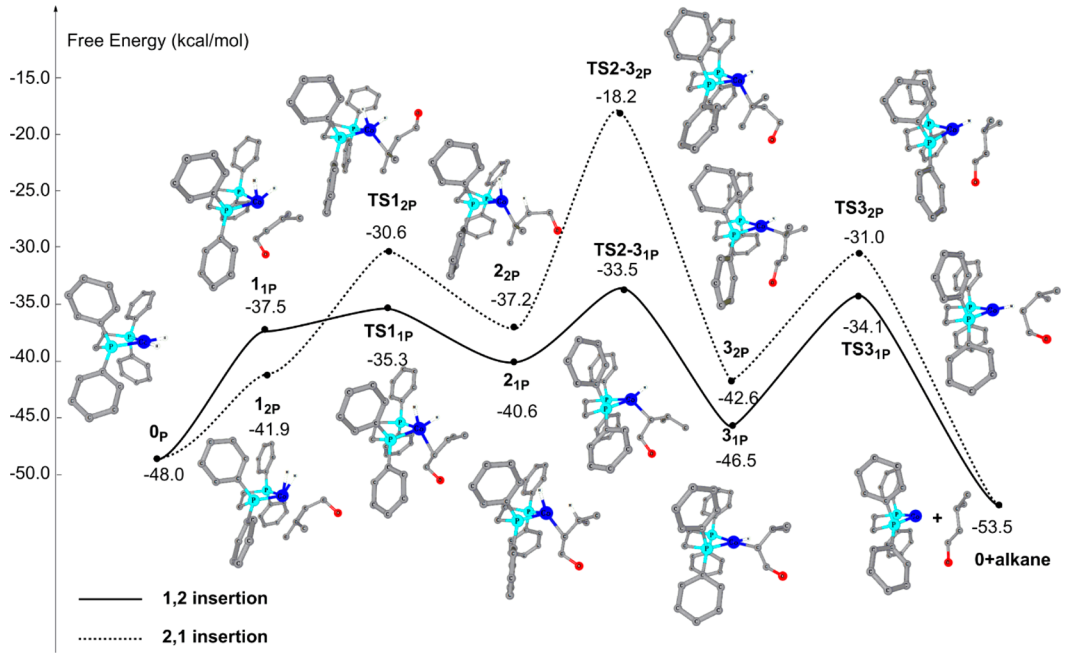

Figure 4. Free energy profiles of reductive elimination mechanism for prenyl alcohol hydrogenation catalyzed by the planar (dppe)CoH_2, $\mathbf{0_P}$ (path 2_P) (H atoms are partly hidden, energy units: kcal/mol).

(diphosphine)$Co(CH_2SiMe_3)_2$ on the quartet state are listed in the Supporting Information.

Alkene Regioselectivity and Reductive Elimination Mechanism. To investigate the unclear catalytic process of alkene hydrogenation catalyzed by (diphosphine)CoH_2, all suitable computational strategies and all possible starting assemblies of bis(phosphine)cobalt complexes have been employed to explore the mechanism of the alkene hydrogenation. 3-Methylbut-2-en-1-ol is the calculated alkene. First, the reductive elimination mechanism was proposed as shown in Figure 2. The catalytic cycle could begin from the vertical $\mathbf{0_T}$, the planar $\mathbf{0_P}$, and bis(phosphine) cobalt(0) complex **0**. An overall mechanism of the alkene hydrogenation with $\mathbf{0_T}$ mainly consists of four steps as shown in Figure 2 (path 1_T in blue): alkene coordination ($\mathbf{0_T} \rightarrow \mathbf{1_T}$), alkene insertion ($\mathbf{1_T} \rightarrow \mathbf{2_T}$), reductive elimination ($\mathbf{2_T} \rightarrow \mathbf{0}$), and catalyst regeneration ($\mathbf{0} \rightarrow \mathbf{0_P}$). The alkene hydrogenation pathway beginning with $\mathbf{0_P}$ is different from the one starting with $\mathbf{0_T}$ as shown in Figure 2 (path 2_P in black). The major differences between path 1_T and path 2_P are in the sequence of the alkene insertion step and the reductive elimination step. The planar $\mathbf{0_P}$ needs an isomerization into the tetrahedral shape (diphosphine)CoH_2 ($\mathbf{1_P}$), which leaves the site for the alkene coordination with Co(II) center. After the insertion of alkene into the Co−H bond to form $\mathbf{2_P}$, the tetrahedral shape changes back to the planar geometric $\mathbf{3_P}$, which is an advantage for the hydrogen transfer to the carbon in the reductive elimination process ($\mathbf{3_P} \rightarrow \mathbf{0}$). Then Co(0) species **0** is obtained, which interacts with the alkane weakly. At last, the catalyst $\mathbf{0_P}$ is regenerated from **0** in the presence of H_2 in a spontaneous exothermic process as shown in Figure S2. The presumed Co(0) cycle starts with **0**, and there are two possible initial steps: the addition of alkene substrate or that of H_2. The former is strongly preferred to give $\mathbf{1^0}$. After alkene coordination, $\mathbf{1^0}$ bonds with H_2 to form $\mathbf{1_P}$ as shown in Figure 2 (path 3_0 in green).

Figures 3 and 4 show the free energy profiles (paths 1_T and 2_P) of prenyl alcohol hydrogenation catalyzed by the vertical $\mathbf{0_T}$ and the planar $\mathbf{0_P}$, respectively, and the modes of alkene insertion into the cobalt−hydride species, 1,2-alkene insertion (anti-Markovnikov addition) and 2,1-alkene insertion (Markovnikov addition), were considered. As shown in Figure 3, prenyl alcohol coordination from $\mathbf{0_T}$ to $\mathbf{1_T}$ is exergonic by 4.0 kcal/mol, and subsequent 1,2-alkene alkene insertion from $\mathbf{1_T}$ to $\mathbf{2_{1T}}$ and 2,1-alkene insertion from $\mathbf{1_T}$ to $\mathbf{2_{2T}}$ are facile steps with low barriers of 0.3 and 2.7 kcal/mol, respectively, which are the regioselectivity-determining steps for alkene hydrogenation catalyzed by the vertical (dppe)CoH_2. Next, hydrogen bonding with Co atoms in $\mathbf{2_{1T}}$ and $\mathbf{2_{2T}}$ transfers to the carbon along with the Co−C bond, and the energy barriers of the reductive elimination step for both the 1,2 insertion pathway and the 2,1 insertion pathway are 11.0 and 10.3 kcal/mol, respectively.

As shown in Figure 4, the C═C bond of prenyl alcohol binds to the tetrahedral shape (diphosphine)CoH_2 to form alkene-coordinated intermediates $\mathbf{1_{1P}}$ and $\mathbf{1_{2P}}$, which are endergonic by 10.5 and 6.1 kcal/mol in 1,2 insertion mode and 2,1 insertion mode, respectively. Subsequent prenyl alcohol insertion in Co−H bond from $\mathbf{1_{1P}}$ to $\mathbf{2_{1P}}$ and from $\mathbf{1_{2P}}$ to $\mathbf{2_{2P}}$ is an accessible step with a barrier of 2.2 and 11.3 kcal/mol, respectively. In consideration of the significant step related to the alkene regioselectivity, the striking energy barrier difference of two modes of alkene insertion implies that 1,2 alkene insertion is preferred in the alkene hydrogenation pathway beginning with $\mathbf{0_P}$ as the same as the process catalyzed by the vertical (dppe)CoH_2, $\mathbf{0_T}$. However, the pathway starting form $\mathbf{0_P}$ contains a geometric rearrangement from $\mathbf{2_P}$ to the planar $\mathbf{3_P}$ with a barrier of 7.1 kcal/mol in the 1,2 insertion pathway and 19.0 kcal/mol in the 2,1 insertion pathway. After undergoing a geometric rearrangement to facilitate hydrogen transfer, the reductive elimination from $\mathbf{3_P}$ to **0** is a slightly difficult step to climb with barriers of 12.4 and 11.6 kcal/mol in the 1,2 insertion pathway and 2,1 insertion pathway, respectively, which is 1.4 and 1.3 kcal/mol higher than the corresponding reductive elimination in alkene hydrogenation pathway

DOI: 10.1021/acs.joc.7b00016
J. Org. Chem. 2017, 82, 2703−2712

beginning with $\mathbf{0_T}$. The rate-determining steps catalyzed by the planar (dppe)CoH_2, $\mathbf{0_P}$, are the reductive elimination with the barrier of 12.4 kcal/mol for the 1,2 insertion pathway and geometric rearrangement with the barrier of 19.0 kcal/mol for the 2,1 insertion pathway, respectively. Therefore, the larger steric hindrance in the 2,1 insertion pathway mainly contributes to the energy-costing geometric rearrangement. As the TOF-determining transition states (TDTS) for the preferred 1,2 insertion mode, the peak $\mathbf{TS2_{1T}}$ in path 1_T is higher than the peak $\mathbf{TS2-3_{1P}}$ in path 2_P on the reductive elimination mechanism. Therefore, path 2_P should be more favorable due to the larger energetic span of path 1_T based on the energetic span model proposed by Shaik et al.[24]

As shown in Figure 5, in the pathway involving **0**, which is generated from reductive elimination of $\mathbf{1Si_P}$ ($\mathbf{2_{1T}}$, $\mathbf{2_{2T}}$, $\mathbf{3_{1P}}$, and $\mathbf{3_{2P}}$) and contains an open coordination site, the catalytic activation could begin with either alkene coordination or H_2 coordination with exergonicity of 17.1 or 15.6 kcal/mol, respectively. Then $\mathbf{1^0}$ undergoes the step of H_2 coordination to form $\mathbf{1_{1P}}$ and $\mathbf{1_{2P}}$, which are endergonic by 12.0 kcal/mol in the 1,2 insertion mode and 7.6 kcal/mol in the 2,1 insertion mode. Therefore, the bis(phosphine)cobalt(0) complex coordinated with substrate could be separated and characterized in the experiment due to thermodynamic stability, which is also regarded as the precatalyst for alkene hydrogenation.[14]

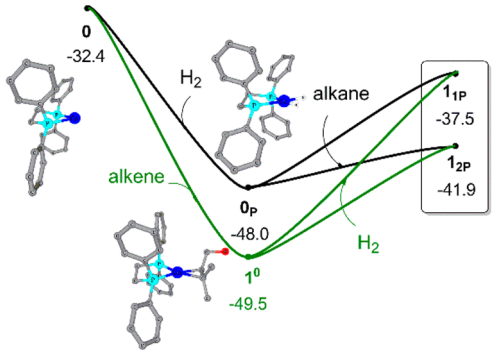

Figure 5. Co(0) species formation and catalytic activation in this system.

σ Bond Metathesis Mechanism. In an attempt to search for the more accessible energy barrier than that of the reductive elimination mechanism, σ bond metathesis mechanism involving H_2 coordination and heterolytic H_2 activation is investigated in the process of prenyl alcohol hydrogenation catalyzed by (dppe)CoH_2, which gives the similar outcome with the reductive elimination followed by oxidative addition.[25] As shown in Figure 6, $\mathbf{21_T}$, $\mathbf{22_T}$, $\mathbf{2_{1P}}$, and $\mathbf{2_{2P}}$ lie on the crossing of the reductive elimination mechanism and σ bond metathesis mechanism, which are followed by the insertion of coordinated alkenes into Co−H bond. After H_2 coordination, $\mathbf{4_{1T}}$, $\mathbf{4_{2T}}$, $\mathbf{4_{1P}}$, and $\mathbf{4_{2P}}$ are obtained, whose strong proton donor character encourages proton transfer to the alkyl group. Then the alkyl group takes the proton and the H- goes to the metal to regenerate the catalyst, which are liberated by heterolytic activation of H_2.

The corresponding free energy profiles of the σ bond metathesis mechanism for prenyl alcohol hydrogenation catalyzed by (dppe)CoH_2 are shown in Figure 7. In the pathway catalyzed by the planar (dppe)CoH_2, the equatorial coordination of H_2 to form $\mathbf{4_{1P}}$ and $\mathbf{4_{2P}}$ is endergonic by 5.5 and 9.5 kcal/mol, respectively. Then H^1 in $\mathbf{4_{1P}}$ and $\mathbf{4_{2P}}$ transfers to the carbon along with the axial Co−C bond with barriers of 8.7 and 7.5 kcal/mol, respectively. The alkane is obtained with planar (dppe)CoH_2 regenerated via $\mathbf{TS4_{1P}}$ and $\mathbf{TS4_{2P}}$, which are largely exergonic by 45.7 and 51.9 kcal/mol, respectively. The rate-determining step of σ bond metathesis mechanism catalyzed by the planar (dppe)CoH_2 of 1,2 insertion mode and 2,1 insertion mode are the H_2 activation step with a barrier of 14.2 and 17.0 kcal/mol, respectively. Similarly, in the pathway catalyzed by the vertical (dppe)CoH_2, the axial coordination of H_2 to form $\mathbf{4_{1T}}$ and $\mathbf{4_{2T}}$ is endergonic by 8.4 and 6.5 kcal/mol, respectively. Then H^1 in $\mathbf{4_{1T}}$ and $\mathbf{4_{2T}}$ transfer to the carbon along with the equatorial Co−C bond with barriers of 4.5 and 9.5 kcal/mol, respectively, and the alkane is obtained with the original vertical (dppe)CoH_2 regenerated via $\mathbf{TS4_{1T}}$ and $\mathbf{TS4_{2T}}$, which are exergonic by 27.7 and 34.0 kcal/mol, respectively. The rate-determining step of the σ bond metathesis mechanism catalyzed by the vertical (dppe)CoH_2 of 1,2 insertion mode and 2,1 insertion mode is the H_2 activation step with barriers of 12.9 and 16.0 kcal/mol, respectively. Similar to the reductive elimination mechanism, 1,2 alkene insertion is preferred in the σ bond metathesis mechanism of alkene hydrogenation catalyzed by both vertical and planar (dppe)CoH_2. However, as the TDTS for preferred 1,2 insertion mode, the energies of $\mathbf{TS4_{1P}}$ and $\mathbf{TS4_{1T}}$ in the σ bond metathesis mechanism are much higher than those of $\mathbf{TS2\text{-}3_{1P}}$ and $\mathbf{TS2_{1T}}$ in reductive elimination mechanism. Therefore, the energetic span of the σ bond metathesis mechanism is larger than that of the reductive elimination mechanism, and the reductive elimination mechanism is still preferred to the σ bond metathesis mechanism in

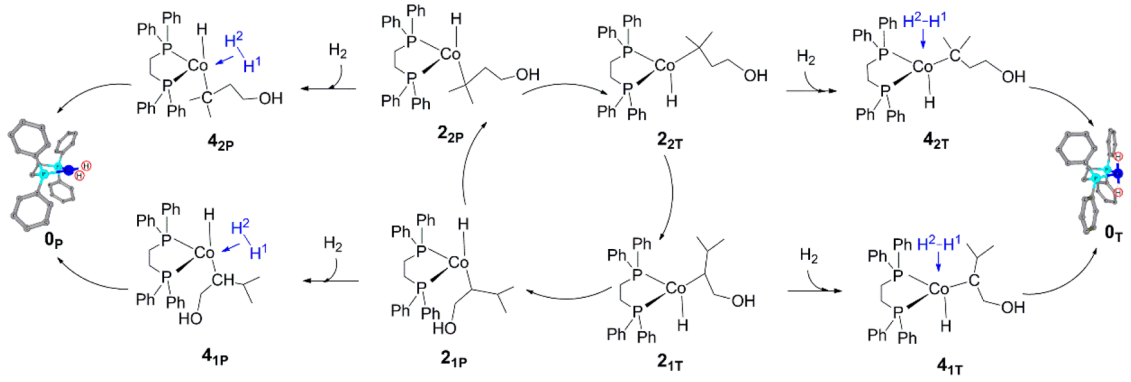

Figure 6. H_2 coordination of σ bond metathesis mechanism.

DOI: 10.1021/acs.joc.7b00016
J. Org. Chem. 2017, 82, 2703−2712

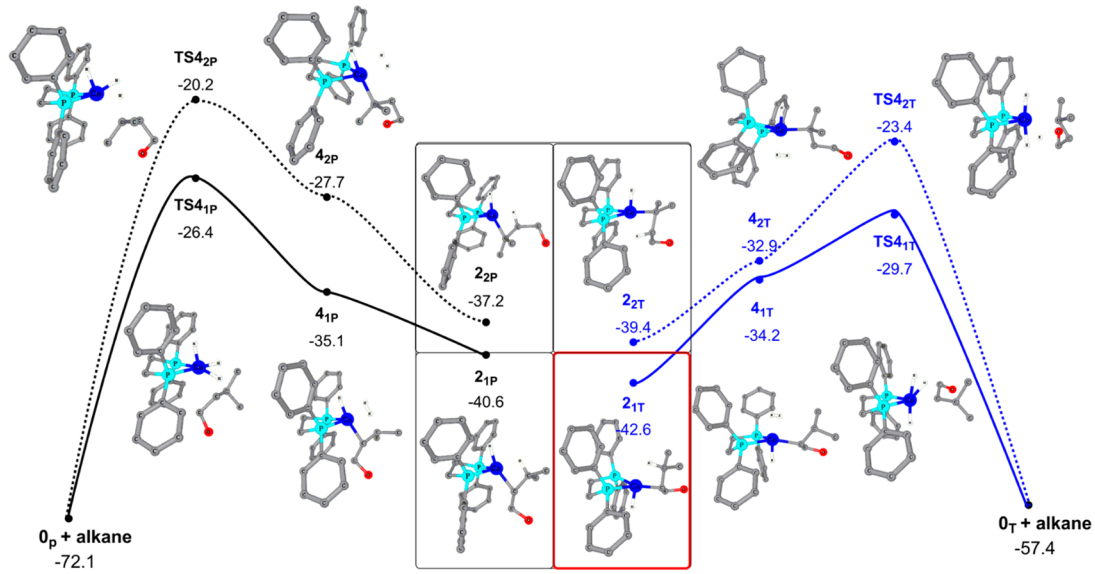

Figure 7. Free energy profiles of σ bond metathesis mechanism for prenyl alcohol hydrogenation catalyzed by (dppe)CoH_2 (H atoms are partly hidden).

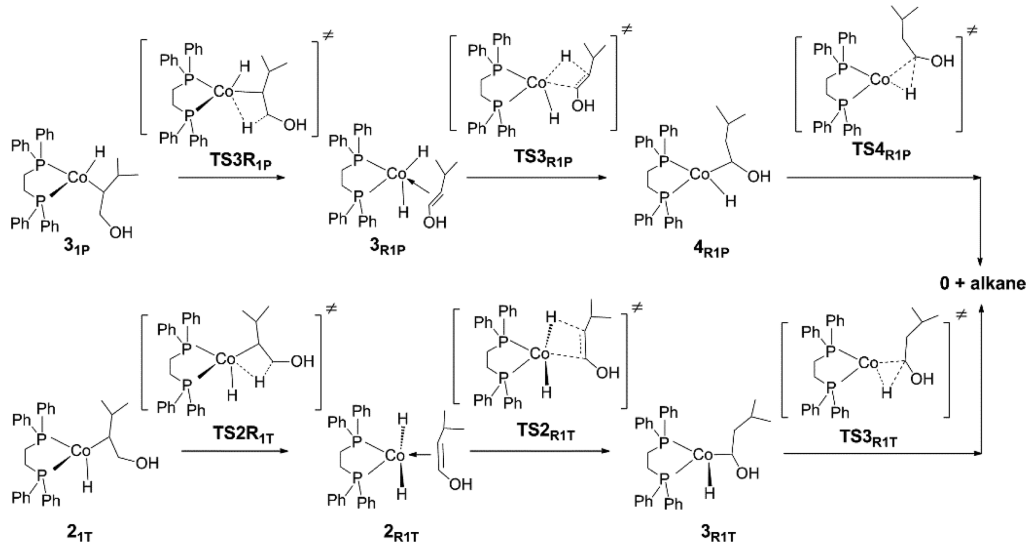

Figure 8. Proposed β hydrogen elimination mechanism starting from and $\mathbf{2_{1T}}$ and $\mathbf{3_{1P}}$.

the favorable 1,2 insertion mode of prenyl alcohol hydrogenation catalyzed by (dppe)CoH_2.

***β* Hydrogen Elimination Mechanism.** Isomerization is often a branched pathway in the alkene hydrogenation, and many transition-metal complexes are capable of catalyzing the 1,3-migration of hydrogen substituents in alkenes, in which there is the net effect of moving the C=C group along the chain of the molecule. Two mechanisms are most commonly found: the first proceeds via alkyl intermediates and the second by η^3-allyls. The second mechanism involves allyl intermediates and is adopted by those metal fragments that have two 2e vacant sites but no hydrides. In our system, the Co−H bond and a vacant site are available for the alkyl route, so the alkyl intermediate may undergo β hydrogen elimination before it has a chance to reductively eliminate. In the six metal−alkyl intermediates ($\mathbf{2_{1T}}$, $\mathbf{2_{2T}}$, $\mathbf{2_{1P}}$, $\mathbf{2_{2P}}$, $\mathbf{3_{1P}}$, and $\mathbf{3_{2P}}$), $\mathbf{3_{1P}}$ and $\mathbf{2_{1T}}$ keep a better balance between the catalytic activation and thermodynamic stability, which are at the crossing of the reductive elimination mechanism and β hydrogen elimination mechanism. As shown in Figure 8, the metal−alkyl intermediates $\mathbf{3_{1P}}$ and $\mathbf{2_{1T}}$ are converted into a hydridemetal alkene complex $\mathbf{3_{R1P}}$ and $\mathbf{2_{R1T}}$ via β hydrogen elimination, which are the reverse of alkene (*E*)-3-methylbut-1-en-1-ol insertion and (Z)-3-methylbut-1-en-1-ol insertion, respectively. In the other alkene insertion manner, (*E*)-3-methylbut-1-en-1-ol inserts in the Co−H bond from $\mathbf{3_{R1P}}$ to $\mathbf{4_{R1P}}$, and (Z)-3-methylbut-1-en-1-ol inserts in the Co−H bond from $\mathbf{2_{R1T}}$ to $\mathbf{3_{R1T}}$. The new metal−alkyl intermediates $\mathbf{4_{R1P}}$ and $\mathbf{3_{R1T}}$ are obtained, which are followed by reductive elimination as the process discussed above.

The corresponding free energy profile of the β hydrogen elimination mechanism starting from $\mathbf{2_{1T}}$ and $\mathbf{3_{1P}}$ is shown in Figure 9. The hydrogen bonding with the βC atom in $\mathbf{2_{1T}}$ transfers to the Co atom along with the Co−αC bond, and the energy barrier of the β hydrogen elimination step is 15.8 kcal/mol, which is exergonic by 16.3 kcal/mol to give $\mathbf{2_{R1T}}$. The corresponding energy barrier of the β hydrogen elimination step from $\mathbf{3_{1P}}$ to $\mathbf{3_{R1P}}$ is 9.5 kcal/mol with an exergonicity of 1.5

DOI: 10.1021/acs.joc.7b00016
J. Org. Chem. 2017, 82, 2703−2712

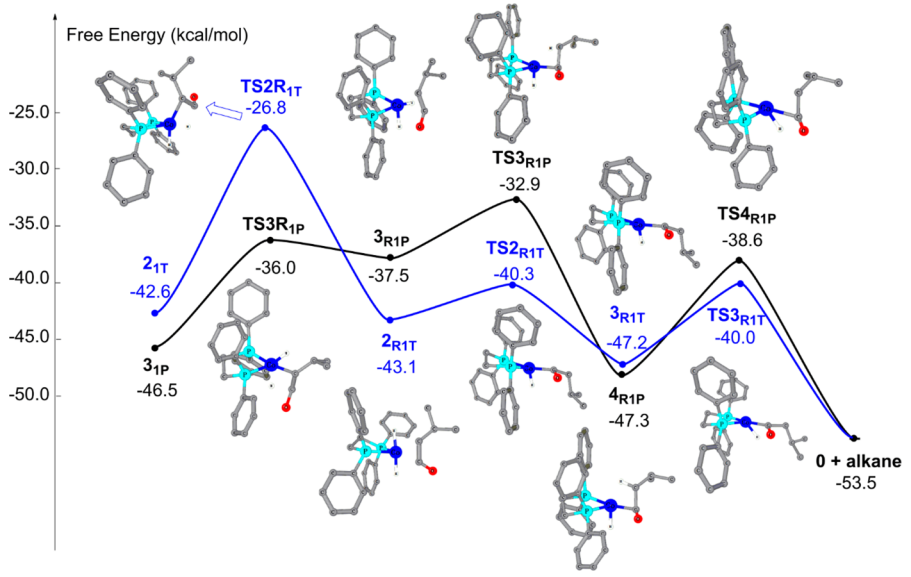

Figure 9. Free energy profiles of β hydrogen elimination mechanism starting from $\mathbf{2}_{1T}$ and $\mathbf{3}_{1P}$ (H atoms are partly hidden).

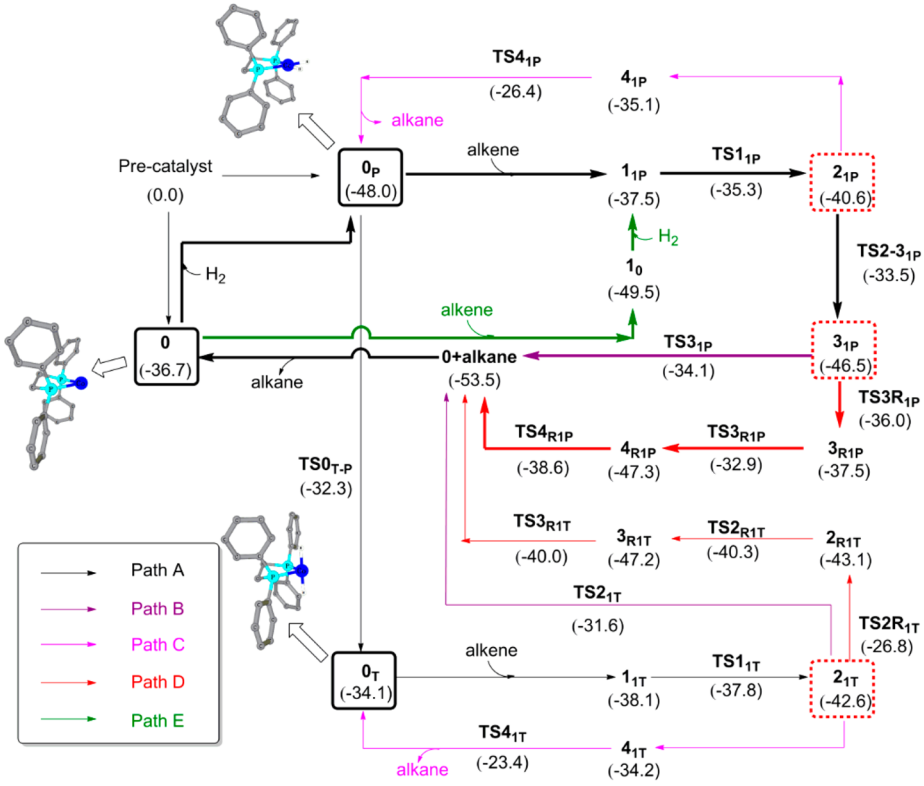

Figure 10. Reaction network of prenyl alcohol hydrogenation catalyzed by bis(phosphine)cobalt dialkyl complex. Path A in black route denotes the pathway of catalytic species formation, path B in purple route denotes the pathway of reductive elimination mechanism, path C in magenta route denotes the pathway of σ bond metathesis mechanism, path D in red route denotes the pathway of β hydrogen elimination mechanism, and path E in green route denotes the Co(0) pathway. The values in parentheses under stationary points are free energies relative to the precatalyst, units: kcal/mol.

kcal/mol. In fact, (*E*)-3-methylbut-1-en-1-ol is easier to generate from $\mathbf{3}_{1P}$ than (*Z*)-3-methylbut-1-en-1-ol from $\mathbf{2}_{1T}$, and subsequent alkene insertions from $\mathbf{2}_{R1T}$ to $\mathbf{3}_{R1T}$ and from $\mathbf{3}_{R1P}$ to $\mathbf{4}_{R1P}$ are facile steps with low barriers of 4.6 and 2.8 kcal/mol, respectively. The energy barriers of reductive elimination from $\mathbf{3}_{R1T}$ and $\mathbf{4}_{R1P}$ to **0** are 7.2 and 8.7 kcal/mol, respectively. Therefore, there is a competition between the β hydrogen elimination with the TOF-determining $\mathbf{TS3}_{R1P}$ of −32.9 kcal/mol and the directly reductive elimination with TOF-determining $\mathbf{TS3}_{1P}$ of −34.1 kcal/mol. The β hydrogen elimination is preferred with the rate-determining barrier of 9.5 kcal/mol from $\mathbf{3}_{1P}$ to $\mathbf{3}_{R1P}$ in the prenyl alcohol hydrogenation catalyzed by planar (dppe)CoH_2. However, the reductive elimination mechanism is still favorable with the TOF-

DOI: 10.1021/acs.joc.7b00016
J. Org. Chem. 2017, 82, 2703−2712

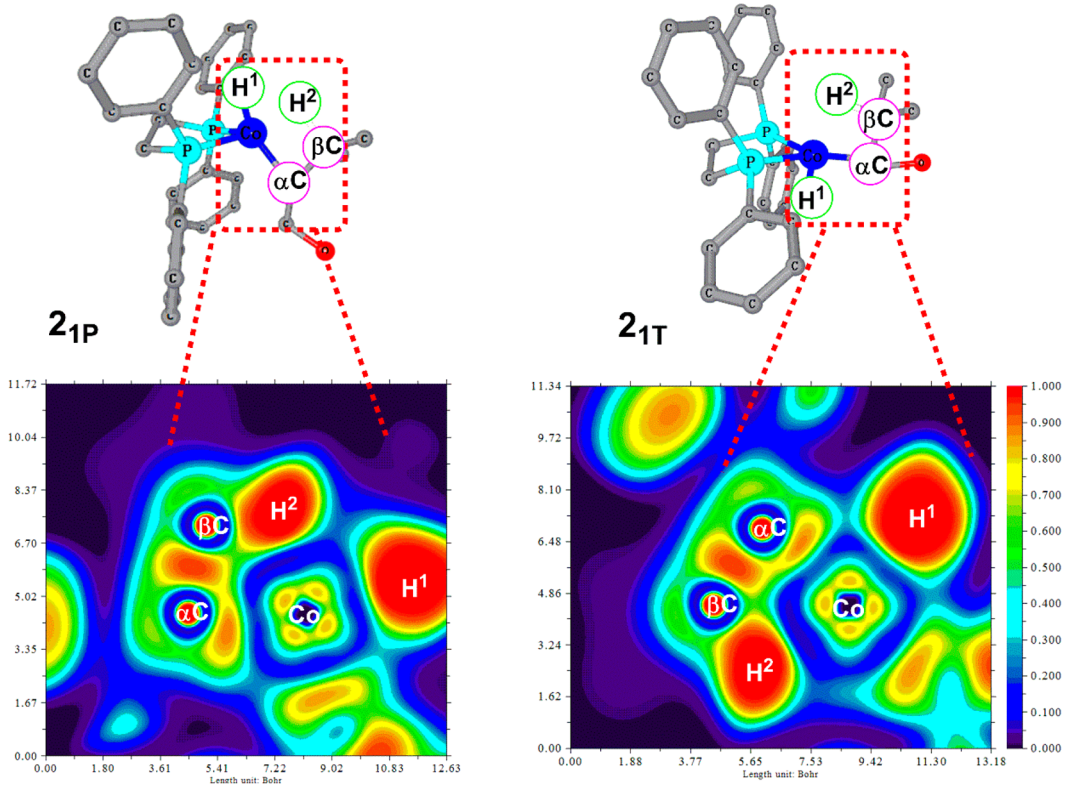

Figure 11. ELF analyses of agostic bond characteristics in $\mathbf{2}_{1P}$ and $\mathbf{2}_{1T}$.

determining $\mathbf{TS2}_{1T}$ of −31.6 kcal/mol in the prenyl alcohol hydrogenation catalyzed by the vertical (dppe)CoH_2.

Preferred Catalytic Activation Process. Taking a panoramic view of different mechanisms based on the calculated results above, the reaction network of prenyl alcohol hydrogenation in the preferred 1,2 alkene insertion mode catalyzed by bis(phosphine)cobalt dialkyl complex is summarized in Figure 10. Path A in the black route denotes the pathway of catalytic species formation, path B in the purple route denotes the pathway of reductive elimination mechanism, path C in the magenta route denotes the pathway of the σ bond metathesis mechanism, path D in the red route denotes the pathway of the β hydrogen elimination mechanism, and path E in the green route denotes the Co(0) pathway. Compound $\mathbf{2}_{1P}$ is at the crossing of paths B and C, $\mathbf{3}_{1P}$ is at the crossing of paths B and D, and $\mathbf{2}_{1T}$ is at the crossing of path B, C, and D. The bold routes denotes the preferred pathway of the catalytic activation process. On account of the free energy profile discussed above, path B (β hydrogen elimination mechanism) and path D (reductive elimination mechanism) starting from $\mathbf{0}_P$ and $\mathbf{0}$ are the preferred competitive pathway in the prenyl alcohol hydrogenation catalyzed by the bis(phosphine)cobalt dialkyl complex. That is, the hydrogenation activity of Co(II) compounds with redox innocent phosphine donors involves Co(0)−Co(II) catalytic mechanisms.

As the crossing points of different mechanisms, it is essential to understand the orientation of the metal−alkyl intermediates. The electron localization functions (ELFs) in the Co−αC−βC plane of $\mathbf{2}_{1P}$ and $\mathbf{2}_{1T}$ are plotted in Figure 11, which clarifies the chemical bonding around cobalt atom using Multiwfn software.[26] The ELF is normalized between 0 (zero localization, blue areas) and 1 (strong localization, red areas) with the value of 1/2 corresponding to a free electron gas behavior. It is observed that the regions with Co−H^2, Co−αC, and Co−βC in $\mathbf{2}_{1P}$ and $\mathbf{2}_{1T}$ are almost the same, which indicates the H^2−βC in $\mathbf{2}_{1P}$ and $\mathbf{2}_{1T}$ bonds to the cobalt center in an agostic fashion rather than classical alkyl mode. Therefore, the H_2 coordination in σ bond metathesis mechanism needs to overcome the electron effects and steric effects of the agostic H^2−βC bond, which could be the origin of the larger energetic span in comparison to the reductive elimination in the prenyl alcohol hydrogenation catalyzed by both the planar and vertical (dppe)CoH_2.

The most obvious difference of the preferred mechanism from different initial active species is that $\mathbf{0}_P$ and $\mathbf{0}$ prefer the β hydrogen elimination mechanism and $\mathbf{0}_T$ prefers to the reductive elimination mechanism. The geometry similarity of transition states is that both $\mathbf{TS2}_{1T}$ and $\mathbf{TS3}_{1P}$ on reductive elimination contain a Co−αC−H^1 three-membered ring, and $\mathbf{TS2R}_{1T}$ and $\mathbf{TS3R}_{1P}$ on β hydrogen elimination contain a Co−αC−βC−H^2 four-membered ring. As shown in Figure 12, the smallest dihedral angles of Co−αC−βC−H^2 in $\mathbf{2}_{1T}$ and $\mathbf{3}_{1P}$ are 49.8° and 45.3°, respectively, and the corresponding

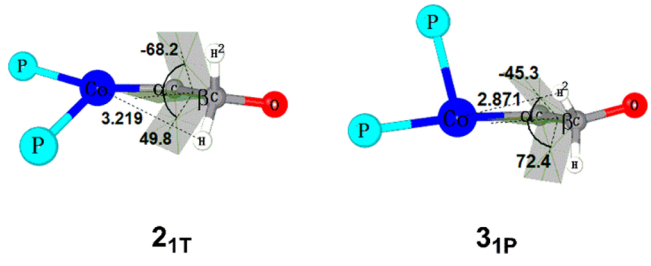

Figure 12. Dihedral angle of Co−αC−βC−H^2 and distance of Co−H^2 in $\mathbf{2}_{1T}$ and $\mathbf{3}_{1P}$. (Only the core parts are displayed.)

DOI: 10.1021/acs.joc.7b00016
J. Org. Chem. 2017, 82, 2703−2712

distances of Co−H^2 in $\mathbf{2_{1T}}$ and $\mathbf{3_{1P}}$ are 3.219 and 2.871 Å, respectively. Therefore, the higher energy barrier of β hydrogen elimination starting from $\mathbf{2_{1T}}$ stems from the larger dihedral angle of Co−αC−βC−H^2 and larger distance of Co−H^2 than that of reductive elimination. However, the larger Co−αC−H^1 ring strain of $\mathbf{TS3_{1P}}$ on reductive elimination contributes to the higher energy barrier than that of β hydrogen elimination. The dihedral angle of Co−αC−βC−H^2, the distance of Co−H^2, and the Co−αC−H^1 ring strain of the $\mathbf{2_{1T}}$ and $\mathbf{3_{1P}}$ determine the preferred catalytic pathway together.

CONCLUSION

The mechanism of directed hydrogenation of hydroxylated alkene catalyzed by bis(phosphine)cobalt dialkyl complexes has been studied by DFT calculations. The active (diphosphine)-CoH_2 with planar structure is most possibly obtained from two successive hydrogenolyses without geometry transformation. The planar dihyride complex $\mathbf{0_P}$ is presumed to be not the only active species in the catalytic reaction, which could transform into the vertical $\mathbf{0_T}$ via $\mathbf{TS0_{T-P}}$ with a barrier of 15.7 kcal/mol on the doublet surface. Co(0) species formation and catalytic activation were confirmed on the quartet state. The experimentally identified and characterized bis(phosphine)-cobalt(0) complex can be accounted for using the pathway involving intermediate **0**. On the basis of the investigation of three different mechanisms (reductive elimination, σ bond metathesis, and β elimination mechanism), the preferred catalytic activation process undergoes the 1,2 alkene insertion mode. $\mathbf{0_P}$ and **0** prefer to the β hydrogen elimination mechanism with a barrier of 9.5 kcal/mol. H_2 coordination in the σ bond metathesis mechanism needs to overcome the electron effects and steric effects of the agostic H^2−βC bond of $\mathbf{2_{1P}}$ and $\mathbf{2_{1T}}$, which is the origin of the larger energetic span in comparison with the reductive elimination. The hydrogenation activity of Co(II) compounds with redox-innocent phosphine donors involves the Co(0)−Co(II) catalytic mechanism.

ASSOCIATED CONTENT

Supporting Information

The Supporting Information is available free of charge on the ACS Publications website at DOI: 10.1021/acs.joc.7b00016.

Cartesian coordinates of optimized geometries and energies of all stationary points along reaction pathways (PDF)

AUTHOR INFORMATION

Corresponding Author

*Phone: 86-10-6444-6598. Fax: 86-10-6444-6598. E-mail: leim@mail.buct.edu.cn.

ORCID

Ming Lei: 0000-0001-5765-9664

Notes

The authors declare no competing financial interest.

ACKNOWLEDGMENTS

This work was supported in part by the National Natural Science Foundation of China (NSFC Grant Nos. 21373023 and 21072018), Beijing Municipal Natural Science Foundation (Grant No. 2162029), and BUCT Fund for Disciplines Construction and Development (Grant No. XK1527). X.M. thanks the China Scholarship Council (CSC) for the CSC scholarship (No. 201406880019). We thank the National Supercomputing Center in Shenzhen (NSCCSZ) and the Special Program for Applied Research on Super Computation of the NSFC−Guangdong Joint Fund (the second phase) for providing part of the computational resources. We especially appreciate Professor Paul J. Chirik and his group member Dr. Max R. Friedfeld at Princeton University for helpful discussions on this system.

REFERENCES

(1) Verendel, J. J.; Pamies, O.; Dieguez, M.; Andersson, P. G. *Chem. Rev.* **2014**, *114* (4), 2130−2169.

(2) Tang, W.; Zhang, X. *Chem. Rev.* **2003**, *103* (8), 3029−3070.

(3) Bullock, R. M. *Science* **2013**, *342* (6162), 1054−1055.

(4) Pregaglia, G.; Andreetta, A.; Ferrari, G.; Ugo, R. *J. Organomet. Chem.* **1971**, *30* (3), 387−405.

(5) Ohgo, Y.; Takeuchi, S.; Natori, Y.; Yoshimura, J. *Bull. Chem. Soc. Jpn.* **1981**, *54* (7), 2124−2135.

(6) Leutenegger, U.; Madin, A.; Pfaltz, A. *Angew. Chem., Int. Ed. Engl.* **1989**, *28* (1), 60−61.

(7) Corma, A.; Iglesias, M.; Del Pino, C.; Sanchez, F. *J. Organomet. Chem.* **1992**, *431* (2), 233−246.

(8) Nindakova, L.; Shainyan, B. *Russ. Chem. Bull.* **2005**, *54* (2), 348−353.

(9) Knijnenburg, Q.; Horton, A. D.; Heijden, H. v. d.; Kooistra, T. M.; Hetterscheid, D. G.; Smits, J. M.; Bruin, B. d.; Budzelaar, P. H.; Gal, A. W. *J. Mol. Catal. A: Chem.* **2005**, *232* (1), 151−159.

(10) (a) Monfette, S.; Turner, Z. R.; Semproni, S. P.; Chirik, P. J. *J. Am. Chem. Soc.* **2012**, *134* (10), 4561−4564. (b) Friedfeld, M. R.; Shevlin, M.; Margulieux, G. W.; Campeau, L.-C.; Chirik, P. J. *J. Am. Chem. Soc.* **2016**, *138*, 3314−3324. (c) Chirik, P. J. *Acc. Chem. Res.* **2015**, *48*, 1687−1695.

(11) (a) Zhang, G.; Scott, B. L.; Hanson, S. K. *Angew. Chem., Int. Ed.* **2012**, *51* (48), 12102−12106. (b) Zhang, G.; Vasudevan, K. V.; Scott, B. L.; Hanson, S. K. *J. Am. Chem. Soc.* **2013**, *135*, 8668−8681.

(12) (a) Lin, T.-P.; Peters, J. C. *J. Am. Chem. Soc.* **2013**, *135*, 15310−1531. (b) Lin, T.-P.; Peters, J. C. *J. Am. Chem. Soc.* **2014**, *136*, 13672−13683.

(13) Friedfeld, M. R.; Shevlin, M.; Hoyt, J. M.; Krska, S. W.; Tudge, M. T.; Chirik, P. J. *Science* **2013**, *342* (6162), 1076−1080.

(14) Friedfeld, M. R.; Margulieux, G. W.; Schaefer, B. M.; Chirik, P. J. *J. Am. Chem. Soc.* **2014**, *136*, 13178−13181.

(15) Trovitch, R. J.; Lobkovsky, E.; Bouwkamp, M. W.; Chirik, P. J. *Organometallics* **2008**, *27*, 6264.

(16) Tokmic, K.; Markus, C. R.; Zhu, L.; Fout, A. R. *J. Am. Chem. Soc.* **2016**, *138* (36), 11907−11913.

(17) Frisch, M. J. et al. *Gaussian 09*, revision B.01; Gaussian, Inc.: Wallingford, CT, 2010.

(18) (a) Becke, A. D. *J. Chem. Phys.* **1993**, *98*, 5648−5652. (b) Lee, C.; Yang, W.; Parr, R. G. *Phys. Rev. B: Condens. Matter Mater. Phys.* **1988**, *37*, 785. (c) Hay, P. J.; Wadt, W. R. *J. Chem. Phys.* **1985**, *82*, 299−310.

(19) (a) Ma, X.; Lei, M.; Liu, S. *Organometallics* **2015**, *34* (7), 1255−1263. (b) Li, L.; Pan, Y.; Lei, M. *Catal. Sci. Technol.* **2016**, *6*, 4450−4457. (c) Feng, R.; Xiao, A.; Zhang, X.; Tang, Y.; Lei, M. *Dalton Trans.* **2013**, *42* (6), 2130−2145. (d) Li, H.; Ma, X.; Lei, M. *Dalton Trans.* **2016**, *45*, 8506−8612. (e) Li, H.; Ma, X.; Zhang, B.; Lei, M. *Organometallics* **2016**, *35* (19), 3301−3310. (f) Lei, M.; Pan, Y.; Ma, X. *Eur. J. Inorg. Chem.* **2015**, *2015* (5), 794−803.

(20) Cioslowski, J. *J. Am. Chem. Soc.* **1989**, *111*, 8333−8336.

(21) (a) Mennucci, B.; Tomasi, J. *J. Chem. Phys.* **1997**, *106*, 5151. (b) Cances, M. T.; Mennucci, B.; Tomasi, J. *J. Chem. Phys.* **1997**, *107*, 3032. (c) Cossi, M.; Barone, V.; Mennucci, B.; Tomasi. *Chem. Phys. Lett.* **1998**, *286*, 253. (d) Tomasi, J.; Persico, M. *Chem. Rev.* **1994**, *94*, 2027.

(22) (a) Sakaki, S.; Ohnishi, Y.; Sato, H. *Chem. Rec.* **2010**, *10*, 29. (b) Ishikawa, A.; Nakao, Y.; Sato, H.; Sakaki, S. *Dalton Trans.* **2010**, *39*, 3279. (c) Ishikawa, A.; Nakao, Y.; Sato, H.; Sakaki, S. *Inorg. Chem.*

DOI: 10.1021/acs.joc.7b00016
J. Org. Chem. 2017, 82, 2703−2712

2009, *48*, 8154. (d) Ohnishi, Y.; Nakao, Y.; Sato, H.; Hiyama, T.; Sakaki, S. *Organometallics* **2009**, *28*, 2583.
(23) (a) Mammen, M.; Shakhnovich, E. I.; Deutch, J. M.; Whitesides, G. M. *J. Org. Chem.* **1998**, *63*, 3821−3830. (b) Zeng, G.; Sakaki, S. *Inorg. Chem.* **2011**, *50* (11), 5290−5297. (c) Zeng, G.; Sakaki, S.; Fujita, K. I.; Sano, H.; Yamaguchi, R. *ACS Catal.* **2014**, *4* (3), 1010−1020.
(24) Kozuch, S.; Shaik, S. *Acc. Chem. Res.* **2011**, *44* (2), 101−110.
(25) Jessop, P. G.; Morris, R. H. *Coord. Chem. Rev.* **1992**, *121*, 155−284.
(26) Lu, T.; Chen, F. J. *J. Comput. Chem.* **2012**, *33*, 580−592.

DOI: 10.1021/acs.joc.7b00016
J. Org. Chem. 2017, 82, 2703−2712